IEEE Access
Multidisciplinary | Rapid Review | Open Access Journal

SPECIAL SECTION ON DATA-ENABLED INTELLIGENCE FOR DIGITAL HEALTH

Received October 30, 2019, accepted November 18, 2019, date of publication November 25, 2019,
date of current version December 9, 2019.

*Digital Object Identifier 10.1109/ACCESS.2019.2955448*

# Three-Dimensional Reconstruction of Abdominal Aortic Aneurysm Based on Compressive Sensing With Iterative Optimization and Its Application in 3D Printing

**XIAOGANG REN[1], YUE WU[1], LEI WANG[1], XIAOQIANG YAN[1], LI ZHANG[1], ZHIYING CAO[1], AND HUANGXING LIN[2]**

[1]Affiliated Changshu Hospital, Soochow University, Changshu 215500, China
[2]Fujian Key Laboratory of Sensing and Computing for Smart City, School of Informatics, Xiamen University, Xiamen 361005, China

Corresponding authors: Xiaogang Ren (icerenx@139.com) and Lei Wang (warmray@163.com)

This work was supported in part by the Jiangsu Committee of Health under Grant H2018071, in part by the Health and Family Planning Commission of Changshu under Grant csws201820, and in part by the Open Fund Project of Jiangsu Key Laboratory of Media Design and Software Technology (Jiangnan University) under Grant 19ST0205.

**ABSTRACT** Three-dimensional reconstruction of abdominal aortic aneurysm is the key technology to improve the success rate of surgical and reduce complications. However, the outer contour of abdominal aortic aneurysm(AAA)is fuzzy, which make it difficult for recent existing method to obtain its accurate segmentation performance and high reconstruction accuracy. In this paper, an improved compressive sensing reconstruction algorithm is proposed, which defines a differentiable and convex total variation (TV) function as an optimization goal function and further reduces the number of projections and improve the quality of reconstructed images. Our proposed algorithm improves the speed and stability of the reconstruction algorithm in three-dimensional reconstruction of abdominal aortic aneurysm. The experimental results show that the proposed model can be used for 3D modeling in 3-D printing to improve the accuracy of endovascular repair and the adaptability of the stent, which is suitable for the application of bioengineering medicine.

**INDEX TERMS** 3-D printing, three-dimensional reconstruction, abdominal aortic aneurysm, compressive sensing, total variation, endovascular repair, computed tomography angiography.

## I. INTRODUCTION

Abdominal aortic aneurysm (AAA) is a common disease amongst middle-aged and elderly people [1]. The main risk is that cancer cells continue to expand and rupture, endangering patients' lives [2]. 90% of abdominal aortic aneurysms occur in the lower part of the renal artery, called as the infrarenal abdominal aortic aneurysm [3]. Although 75% of abdominal aortic aneurysms do not show significant clinical symptoms, the patient's mortality rate is as high as 78%-94% once they rupture. The characteristic geometric parameters of AAA, including the maximum diameter, the length of the tumor, the diameter of the aneurysmal neck and the length of the aneurysmal neck, have all been recommended as important indicators for judging whether AAA is broken, but the correlation between these geometric parameters and AAA rupture is not accurate [4]. For example, the largest diameter of abdominal aortic aneurysm is often used as the basis for judging whether the AAA rupture is present (male patients with a tumor diameter >5.5cm and female patients with a tumor diameter >5cm). However, in fact, there is a phenomenon where some small-diameter abdominal aortic aneurysms rupture and large-diameter tumors have not ruptured [5], [6]. Therefore, the accuracy of detection using only geometric features is not high.

However, the geometric characteristic parameters of AAA are very important for the formulation of AAA surgical procedures. At present, endovascular repair (EVAR) is the most common method for the treatment of abdominal aortic aneurysms [7]. When making the surgical plan, doctors need to use CT images to measure some characteristic geometric parameters of AAA, such as aneurysmal neck diameter,

The associate editor coordinating the review of this manuscript and approving it for publication was Yongtao Hao.

length of tumors, etc. to determine the appropriate type, length, location of EVAR stent, and so on. Geometric parameters of abdominal aortic aneurysms are closely related to a series of complications, including endoleak, stent lateral displacement, aneurysm growth and final rupture [8]. Accurate measurement of geometric parameters is of great significance in preventing complications after EVAR.

Three-dimensional reconstruction of abdominal aortic aneurysm is the key technology to improve the success rate of surgical and reduce complications [9]. Obtaining the internal and external contours of the abdominal aortic aneurysm on the computed tomography angiography (CTA) image sequence is the premise for accurate measurement and research of the tumor, and also provides a reliable basis for clinical diagnosis. With the development of computer image processing technology, image segmentation technology has been widely used in medical image processing [10]. Nowadays, segmentation and modeling of vascular lumen have been realized. In recent years, according to three-dimensional volume data, regional growth and level set and the graph cutting method are adopted to realize the three-dimensional segmentation of the significant object [11]. However, the outer contour of the abdominal aortic aneurysm is relatively low, and the existing three-dimensional segmentation method cannot be used to obtain accurate segmentation results. The accurate segmentation of the outer contour of the tumor mainly depends on manual operation of radiologist, so the continuous automatic segmentation of the outer contour of abdominal aortic aneurysm in the CTA image sequence is of great research significance and application value [12]. The level set method based on the local binary fitting (LBF) model makes full use of the gray level information in the neighborhood of the evolution curve, which is suitable for the segmentation of fuzzy contours [13], [14]. Based on the LBF level set, combined with context information and narrow-band constraints, the high-precision automatic segmentation of the abdominal aortic aneurysm in the image sequence is realized [16].

High-level image information is a common method in fuzzy target segmentation. Reference [15] combined with principal component analysis and K-Means to achieve segmentation of different aortic aneurysm segmentation, which is suitable for medical image segmentation of specific components with different brightness. In the segmentation of abdominal aortic aneurysm, the outer contour can not be obtained only by the brightness information. Reference [17] uses the active contour model to realize liver segmentation in CT images, which requires a large number of samples in the early stage of training, and the selection of samples is required for fuzzy medical images. In addition, the shape of the abdominal aortic aneurysm is usually added to the shape prior. Reference [18] use the elliptical model for outer contour segmentation. Reference [8] analyze the gray histogram and morphological characteristics of the abdominal aortic aneurysm area to segment the internal and external contours. Reference [12] added geometric constraints to the thrombus and ectal segmentation of abdominal aortic aneurysms. These simple shape-based methods are applied to the outer contour segmentation of normal aorta and partial tumor slices. The formation of the thrombus causes the outer contour to be not similar to the ellipse or the inner and outer contours, and the method is limited to a specific geometry or lumen contour and cannot segment accurately the three-dimensional reconstruction of abdominal aortic aneurysm.

Since 3D reconstruction is mathematically a solution to the inverse problem of the typical ill-posedness problem, the solution of the ill-posedness problem is often performed using a regularization method. Compressive sensing(CS) theory points out that if a signal is compressible under known orthogonal basis, or sparse in a certain transform domain, then the observation matrix can be used to project the high-dimensional signal onto the low-dimensional and then the original signal can be restored by optimizing the problem [19]. CS theory also believes that the sampling rate depends on the sparsity and non-correlation of the data. In theory, any signal can be compressed as long as it has the proper sparse basis. In this paper, the compressive sensing algorithm is improved and optimized to further reduce the number of projections and improve the quality of reconstructed images. An improved compressive sensing reconstruction algorithm is proposed, which defines a differentiable and convex total variation (TV) function as an optimization goal function and further reduces the number of projections and improve the quality of reconstructed images. Our proposed algorithm improves the speed and stability of the reconstruction algorithm in three-dimensional reconstruction of abdominal aortic aneurysm.

## II. MATERIALS AND METHODS

### A. MATERIALS

To obtain a three-dimensional reconstruction model, segmentation of the abdominal aortic aneurysm is required. The anatomical structure of an abdominal aortic aneurysm is composed of inner and outer walls, and thrombus between them. The cross-sectional structure and outer contour of the abdominal aortic aneurysm are shown in Fig.1. It can be seen from Fig. 1 that the tumors are closely connected with the surrounding tissues on different sections of the sequence, and the peripheral tissues and intratumoral thrombus are close in brightness which makes the loss of part of the outer contour section. The intratumoral cavity is complex and not similar to the outer contour under the influence of intracavitary thrombus, which leads to low gradient differences at the boundary of the outer wall and other neighboring structures.. Therefore, the precise segmentation of the outer contour on high blur or even partial loss image is the main solution that needs to solve problem. Once the segmentation result is obtained, an efficient reconstruction algorithm is needed for three-dimensional reconstruction [20].

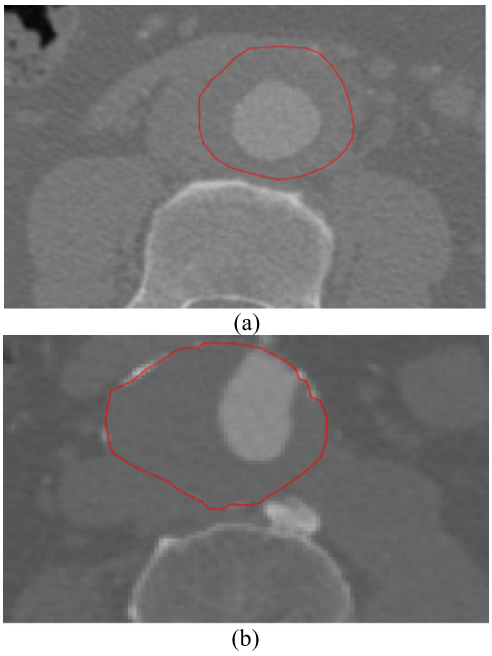

**FIGURE 1.** The composition of AAA and its outer contour; (a) AAA with round shape (b) AAA with oval shape.

### B. THE IMPROVED COMPRESSIVE SENSING ALGORITHM

In this paper, an improved Compressive Sensing (CS) reconstruction algorithm is proposed to improve the reconstruction accuracy of complex structures in AAA, which achieves good quality of the reconstructed image by using a very small number of projections. The compressive sensing reconstruction algorithm defines a total variation function with differentiable convex as the optimization objective, which improves the speed and stability of finite difference transform calculation [20]. In addition, the maximum likelihood expectation maximization (MLEM) algorithm is proposed as the Projection on Convex Set (POCS) process of CS. The POCS process of traditional compressive sensing algorithm is implemented by ART algorithm. The access mode of projection data and the selection of relaxation factor of ART algorithm will affect the number of iterations and the quality of reconstructed image [18]. These two parameters are closely related to the number of projections and image features, which are usually difficult to determine. The improved CS algorithm proposed in this paper uses MLEM as its POCS process to avoid such problems. On the basis of theoretical analysis, real experiments were carried out with CT scanning, and the reconstruction effects are compared and evaluated [21].

Because of the characteristics of biological tissues, the changes of tissues in the same organ will not be great under normal conditions. The image has the characteristics of local smoothness, so it can be considered that its finite difference image is sparse. Experiments also show that the finite difference of biological projection image has good sparsity and can reflect the edge information of the image [22]. Therefore, the finite difference transformation (FDT) is used as its sparse transformation, and the norm$l_1$of FDT, namely total variation (TV), is used as the optimization objective function.

Two-dimensional total variation is defined as:

$$TV\ (F) = \int_{\Omega} \sqrt{|\nabla F|^2} dxdy = \int_{\Omega} \sqrt{|\partial F/\partial y|^2} dxdy \tag{1}$$

This function is non-convex and non-differentiable. The speed and stability of solving non-convex functions are worse than that of convex functions. In this paper, we transform the two-dimensional total variation into another form, which is shown as follows:

$$\begin{aligned} TV\ (F) &= \int_{\Omega} \sqrt{|\nabla F|^2} \\ dxdy &= \int_{\Omega} \sqrt{|\partial F/\partial x|^2} dxdy + \int_{\Omega} \sqrt{|\partial F/\partial y|^2} dxdy \end{aligned} \tag{2}$$

For two-dimensional images, FDT can be defined as:

$$TV\ (F) = \sum_{i,j} \left( \sqrt{\left(f_{i,j} - f_{i-1,j}\right)^2} + \sqrt{\left(f_{i,j} - f_{i-1,j}\right)^2} \right) \tag{3}$$

Then, image F is reconstructed by solving the following optimization problem:

$$\min TV\ (F), \quad s.t. P = AF,\ F \geq 0 \tag{4}$$

where, P is a transmission projection image; A is observation matrix; F is a reconstructed image. Constraint $P = AF$ is solved by Projection on Convex Set (POCS), and optimization problem is solved by gradient descent method (GDM). For the scanning mode of optical CT, the measurement matrix satisfies the RIP characteristics. Therefore, the reconstruction of sparsely sampled signals has a stable solution. The specific calculation process consists of two steps, one is the MLEM process under constraints, and the other is the solution of TVM (Total Variation Minimization) process.

*Step 1:* the POCS (Project on Convex Set) process with constraint $P = AF$ is shown as follows:

(1) Initialize the reconstructed image, shown as follows

$$f^0_{MLEM}\ (k = 0) = 0 \tag{5}$$

where k is the total number of iterations.

(2) Using MLEM iterative image, we can obtain as the following equation,

$$f_j^{(k+1)} = f_j^{(k)} \frac{1}{\sum\limits_i a_{i,j}} \sum_i a_{i,j} \frac{p_i}{\sum\limits_i a_{i,j} f_l^{(k)}} \tag{6}$$

where, k is the total number of iterations; $f_j^k$is the estimated value after k iterations; $p_i$ is the i-th ray projection value; and $a_{i,j}$ represents the probability that photons emitted from the object pixel$j$will be detected by the i-th unit of the detector.

(3) Calculate the value of the following equation with non-negative constraint:

$$F_{MLEM}\ (k) = \begin{Bmatrix} F_{MLEM}\ (k), & F_{MLEM}\ (k) \geq 0 \\ 0, & F_{MLEM}\ (k) < 0 \end{Bmatrix} \tag{7}$$

*Step 2:* TVM process

(1) Initialize the TVM image

$$F^0_{TVM}(k) = F_{POCS}(k) \tag{8}$$

(2) Calculate the incremental factor

$$d(k) = \left\| X^0_{MLEM}(k) X_{POCS}(k) \right\| \tag{9}$$

(3) Calculate the gradient and direction of total variation

$$\vec{G}^{n-1}(k) = \frac{\partial \|F\|_{TV}}{\partial f_{i,j}} \Big|_{F=F^{n-1}_{TVN}(k)}, \quad \hat{G}^{n-1}(k) \frac{\hat{G}^{n-1}(k)^{n-1}(k)}{\left|\vec{G}^{m-1}(k)\right|} \tag{10}$$

where $n\,(1 < n < N)$ is the iteration number.

(4) Correct the image in negative direction of gradient

$$F^m_{TVM}(k) = F^{m-I}_{TVM}(k) - \lambda d_A(k) \hat{G}^{n-1}(k), \quad n = n+1 \tag{11}$$

where, $\lambda$ is regulation factor.

(5) If the calculation results satisfy the following condition

$$\left\| F^k_{POCS}(k) - F^{K-1}_{POCS}(k) \right\| < \varepsilon \tag{12}$$

where $\varepsilon$is an arbitrarily small positive number, the algorithm terminates.

Otherwise,

$$F^0_{MLEM}(k+1) = F^N_{TVM}(k) \tag{13}$$

and run the next iteration.

## III. EXPERIMENTAL ANALYSIS AND ITS APPLICATION IN 3D PRINTING

### A. EXPERIMENTAL PLATFORM AND EVALUATION INDEX

The experimental software environment is 64-bit Mat1ab2013a, and the hardware environment is a computer equipped with Core i5-3320 2.60 GHz and 8 GB memory. The experimental data is the abdominal LTA image sequence data set of the two groups of abdominal aortic aneurysm patients. The image resolution is 512 ×512, and the corresponding spatial resolution is 0. 628 mm × 0. 628 mm and 0.646 5 mm×0.646 5 Mm[27].

The average value of DICE score, Jaccard and volume overlap error (VOE), relative volume difference (RVD), average symmetric surface distance (ASSD) and maximum symmetric surface distance (MSSD) are used in this paper to evaluate the segmentation performance of abdominal aortic aneurysm [24].

### B. QUALITATIVE AND QUANTITATIVE ANALYSIS

The traditional level set method and the graph-cut method are used to perform the comparison analysis of the extracorporeal contours segmentation on the single layer LTA image [25]. The segmentation results are shown in Fig. 2. Fig. 2(a) is the original image. The Snake segmentation method uses a randomly generated initialization curve. Figure 2(c) uses a horizontal set segmentation method based on local region information and shape constraints [6]. Figure 2(d) uses a binary level set based on LBF [26]. Method. Figure 2(e) is the result of our proposed method. The experiment selects the same LTA slice, Figure 2(b) uses global initialization, and Figure 2 (c-e) uses the same level set to initialize the outline and width. Table 1 is the quantitative segmentation results of different segmentation models. It can be seen that the proposed model can accurately segment the outer and inner contours in AAA.

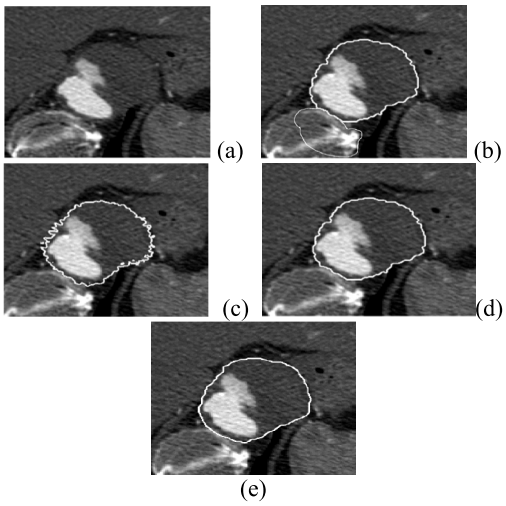


**FIGURE 2.** The segmentation results by different method.(a)original image; (b)Snake; (c)literature [6]; (d)LBF; (e)Proposed method.

**TABLE 1.** Average evaluation indicators of different models.

| Models | Dice | VOE | RVD | ASSD | MSSD |
|---|---|---|---|---|---|
| Snake | 0.841 | 0.112 | 0.021 | *3.028* | *41.188* |
| Literature[6] | 0.838 | 0.111 | 0.011 | 4.860 | 48.301 |
| LBF | 0.821 | 0.110 | 0.024 | 3.487 | 42.110 |
| Proposed method | 0.870 | 0.078 | 0.006 | 1.821 | 31.183 |

### C. THREE-DIMENSIONAL RECONSTRUCTION AND ITS APPLICATION IN 3D PRINTING

Once the segmentation result is obtained, an efficient reconstruction algorithm is needed for three-dimensional reconstruction. CTA image is used as the experimental model. Projections from 360, 180, 90, 60, 30 and 18 angles are carried out within 360 degrees. Then FBP algorithm and improved CS algorithm are used to reconstruct the projected image. FBP algorithm is an analytical algorithm. Because of its clear concept and fast reconstruction speed,

**TABLE 2. Quality comparison and evaluation of reconstructed images.**

| Algorithm | RMSE | PSNR | SSIM |
|---|---|---|---|
| Proposed | 3.49 | 21.87 | 0.85 |
| FBP | 9.15 | 17.56 | 0.43 |

the reconstructed image of its dense angle projection is often used as the criterion to evaluate other algorithms.

The reconstruction result of FBP from various angles and the reconstruction result of our proposed algorithm are analyzed in experiment. It can be seen intuitively that when the number of projections is more than 150, the quality of reconstructed image of FBP algorithm is not significantly different from that of our proposed algorithm; when the number of projections is less than 90, the reconstructed image of filtered back-projection algorithm has obvious artifacts, while our proposed algorithm has better image quality; when the number of projections is less than 40, it is difficult for both algorithms to achieve better reconstruction results. Therefore, 40 reconstructed images are used for comparison and evaluation [28].

In order to accurately compare the difference between the reconstructed image and the original image, we use vertical and horizontal central sections as comparison objects. In our experiment analysis, the reconstructed image using the improved our proposed algorithm is very close to the original image, while the reconstructed image based on FBP algorithm is quite different from the original image and has obvious artifacts.

As can be seen from Table 2, the improved our proposed algorithm can obtain better reconstruction results at 40 sparse projection angles. Next, we use CTA to scan, and use the improved our proposed algorithm to reconstruct. According to the experiment results, FBP algorithm has obvious artifacts in 90 projection angles, and the proposed algorithm has a very good reconstruction quality in 40 angles. Different from the simulation, CS algorithm uses the actual scanned image to reconstruct. When CS algorithm has less than 40 angles, the quality of reconstruction cannot meet the actual application requirements. Therefore, the projections from less than 40 angles should not be adopted in practical applications.

### D. DISCUSSION

Most of the AAA is associated with intratumoral thrombosis, and the mechanical effects of intracavitary thrombosis on AAA are currently controversial. Because of the presence of thrombus in the clinical rupture of the tumor, some scholars believe that the presence of thrombus will lead to the degeneration of the AAA wall, which in turn reduces the strength of the tumor wall. It has also been suggested that blood flow can be transmitted to the wall of the tumor through loose porous wall thrombus, resulting in increased pressure on the wall of the tumor. These factors can lead to an increase in the growth rate of AAA tumors and an increased risk of rupture. Some scholars further compared the effects of the thrombus on the anterior and posterior parts of the tumor on the growth of the tumor. The results showed that the thrombus in the front of the tumor had a stress on the vessel wall that was larger than that in the posterior part of the tumor [27]. The former has a faster growth rate of the tumor diameter than the latter. However, some studies have suggested that the presence of intracavitary thrombosis is protective against AAA, which can alleviate the stress on the tumor wall and thus reduce the risk of AAA rupture. The effect of endovascular thrombus on the rupture of AAA remains to be further studied, but the addition of true thrombus information to the AAA model will certainly help to improve the authenticity of the simulation results. In addition, because there are large differences in the composition and microstructure of thrombus between different individuals, obtaining individualized thrombus data can simulate more accurate results. Therefore, our proposed compressed sensing 3D reconstruction method uses this prior information to improve the reconstruction accuracy. In particular, there is no subsequent 3D printed structural support structure, which has better adaptability.

## IV. CONCLUSION

Three-dimensional reconstruction of abdominal aortic aneurysm is the key technology to improve the success rate of surgical and reduce complications. However, the outer contour of abdominal aortic aneurysm(AAA)is fuzzy, which make it difficult for recent existing method getting its accurate segmentation performance and high reconstruction accuracy. In this paper, an improved compressive sensing reconstruction algorithm is proposed, which defines a differentiable and convex total variation (TV) function as an optimization goal function and further reduces the number of projections and improve the quality of reconstructed images. Our proposed algorithm improves the speed and stability of the reconstruction algorithm in three-dimensional reconstruction of abdominal aortic aneurysm. The experimental results show that the proposed model can be used for 3D modeling in 3-D printing to improve the accuracy of endovascular repair and the adaptability of the stent.

## REFERENCES

[1] T. Siriapisith, W. Kusakunniran, and P. Haddawy, "Outer wall segmentation of abdominal aortic aneurysm by variable neighborhood search through intensity and gradient spaces," *J. Digit. Imag.*, vol. 31, no. 4, pp. 490–504, 2018.

[2] Y. Zha, G. Peng, L. Li, C. Yang, X. Lu, and Z. Peng, "Quantitative aortic distensibility measurement using CT in patients with abdominal aortic aneurysm: Reproducibility and clinical relevance," *BioMed Res. Int.*, vol. 2017, Apr. 2017, Art. no. 5436927.

[3] J. T. Boersen, L. H. van den Ham, J. M. Heyligers, A. C. Vahl, P. W. Vriens, M. M. Reijnen, and J. P. de Vries, "Validation of preprocedural aortic aneurysm volume calculations to estimate procedural fill volume of endobags in endovascular aortic sealing," *J. Cardiovascular Surg.*, vol. 58, no. 5, pp. 674–679, 2017.

[4] T. Hagerty, P. Geraghty, and A. C. Braverman, "Abdominal aortic aneurysm in marfan syndrome," *Ann. Vascular Surgery*, vol. 40, pp. 294.e1–294.e6, Apr. 2017.
[5] C. Villard and R. Hultgren, "Abdominal aortic aneurysm: Sex differences," *Maturitas*, vol. 109, pp. 63–69, Mar. 2018.
[6] S. P. Roddy, "Abdominal aortic aneurysm screening," *J. Vascular Surg.*, vol. 65, no. 5, p. 1537, 2017.
[7] H. Mohammadi, S. Lessard, E. Therasse, R. Mongrain, and G. Soulez, "A numerical preoperative planning model to predict arterial deformations in endovascular aortic aneurysm repair," *Ann. Biomed. Eng.*, vol. 46, no. 12, pp. 2148–2161, 2018.
[8] J. J. Siracuse, B. M. Krafcik, A. Farber, J. A. Kalish, A. McChesney, D. Rybin, G. Doros, and M. H. Eslami, "Contemporary open repair of ruptured abdominal aortic aneurysms," *J. Vascular Surg.*, vol. 65, no. 4, pp. 1023–1028, 2017.
[9] K. Tzirakis, Y. Kamarianakis, E. Metaxa, N. Kontopodis, C. V. Ioannou, and Y. Papaharilaou, "A robust approach for exploring hemodynamics and thrombus growth associations in abdominal aortic aneurysms," *Med. Biol. Eng. Comput.*, vol. 55, no. 8, pp. 1493–1506, 2017.
[10] G. T. Jones *et al.*, "Meta-analysis of genome-wide association studies for abdominal aortic aneurysm identifies four new disease-specific risk loci," *Circulat. Res.*, vol. 120, no. 2, pp. 341–353, 2017.
[11] O. Stackelberg, A. Wolk, K. Eliasson, A. Hellberg, A. Bersztel, S. C. Larsson, N. Orsini, A. Wanhainen, and M. Björck, "Lifestyle and risk of screening-detected abdominal aortic aneurysm in men," *J. Amer. Heart Assoc.*, vol. 6, no. 5, 2017, Art. no. e004725.
[12] I. Isgum, M. Staring, A. Rutten, M. Prokop, M. A. Viergever, and B. van Ginneken, "Multi-atlas-based segmentation with local decision fusion—Application to cardiac and aortic segmentation in CT scans," *IEEE Trans. Med. Imag.*, vol. 28, no. 7, pp. 1000–1010, Jul. 2009.
[13] Y. Zheng, M. John, R. Liao, A. Nottling, J. Boese, J. Kempfert, T. Walther, G. Brockmann, and D. Comaniciu, "Automatic aorta segmentation and valve landmark detection in C-Arm CT for transcatheter aortic valve implantation," *IEEE Trans. Med. Imag.*, vol. 31, no. 12, pp. 2307–2321, Dec. 2012.
[14] Y. Zheng, M. John, R. Liao, J. Boese, U. Kirschstein, B. Georgescu, S. K. Zhou, J. Kempfert, T. Walther, G. Brockmann, and D. Comaniciu, "Automatic aorta segmentation and valve landmark detection in C-Arm CT: Application to aortic valve implantation," in *Proc. Int. Conf. Med. Image Comput. Comput.-Assist. Intervent.* New York, NY, USA: Springer-Verlag, 2010, pp. 476–483.
[15] S. D. Olabarriaga, J. M. Rouet, M. Fradkin, M. Breeuwer, and W. J. Niessen, "Segmentation of thrombus in abdominal aortic aneurysms from CTA with nonparametric statistical grey level appearance modeling," *IEEE Trans. Med. Imag.*, vol. 24, no. 4, pp. 477–485, Apr. 2005.
[16] M. de Bruijne, B. van Ginneken, W. J. Niessen, J. B. A. Maintz, and M. A. Viergever, "Active-shape-model-based segmentation of abdominal aortic aneurysms in CTA images," *Proc. SPIE*, vol. 4684, no. 2, p. 127, 2002.
[17] A. Herment, N. Kachenoura, M. Lefort, M. Bensalah, A. Dogui, F. Frouin, E. Mousseaux, and A. De Cesare, "Automated segmentation of the aorta from phase contrast MR images: Validation against expert tracing in healthy volunteers and in patients with a dilated aorta," *J. Magn. Reson. Imag.*, vol. 31, no. 4, pp. 881–888, 2010.
[18] Z. Tang, S. Wang, J. Huo, H. Guo, H. Zhao, and Y. Mei, "Bayesian framework with non-local and low-rank constraint for image reconstruction," *J. Phys. Conf. Ser.*, vol. 787, Jan. 2017, Art. no. 012008.
[19] Y. Jiang, D. Wu, Z. Deng, P. Qian, J. Wang, G. Wang, F.-L. Chung, K.-S. Choi, and S. Wang, "Seizure classification from EEG signals using transfer learning, semi-supervised learning and TSK fuzzy system," *IEEE Trans. Neural Syst. Rehabil. Eng.*, vol. 25, no. 12, pp. 2270–2284, Dec. 2017.
[20] Y. Jiang, Z. Deng, F.-L. Chung, G. Wang, P. Qian, K.-S. Choi, and S. Wang, "Recognition of epileptic EEG signals using a novel multiview TSK fuzzy system," *IEEE Trans. Fuzzy Syst.*, vol. 25, no. 1, pp. 3–20, Feb. 2017.
[21] Y. Jiang, F.-L. Chung, S. Wang, Z. Deng, J. Wang, and P. Qian, "Collaborative fuzzy clustering from multiple weighted views," *IEEE Trans. Cybern.*, vol. 45, no. 4, pp. 688–701, Apr. 2015.
[22] K. Xia, H. Yin, P. Qian, Y. Jiang, and S. Wang, "Liver semantic segmentation algorithm based on improved deep adversarial networks in combination of weighted loss function on abdominal CT images," *IEEE Access*, vol. 7, pp. 96349–96358, 2019.
[23] K.-J. Xia, H.-S. Yin, and Y.-D. Zhang, "Deep semantic segmentation of kidney and space-occupying lesion area based on SCNN and ResNet models combined with SIFT-flow algorithm," *J. Med. Syst.*, vol. 43, no. 1, pp. 2:1–2:12, 2019.
[24] U. Tariq, A. Hsiao, M. Alley, T. Zhang, M. Lustig, and S. S. Vasanawala, "Venous and arterial flow quantification are equally accurate and precise with parallel imaging compressed sensing 4D phase contrast MRI," *J. Magn. Reson. Imag.*, vol. 37, no. 6, pp. 1419–1426, 2013.
[25] Y. Kwak, S. Nam, M. Akçakaya, T. A. Basha, B. Goddu, W. J. Manning, V. Tarokh, and R. Nezafat, "Accelerated aortic flow assessment with compressed sensing with and without use of the sparsity of the complex difference image," *Magn. Reson. Med.*, vol. 70, no. 3, pp. 851–858, 2013.
[26] P. T. Boufounos and R. G. Baraniuk, "1-Bit compressive sensing," in *Proc. 42nd Annu. Conf. Inf. Sci. Syst.*, Mar. 2008, pp. 16–21.
[27] H. Gan, Z. Li, J. Li, X. Wang, and Z. Cheng, "Compressive sensing using chaotic sequence based on Chebyshev map," *Nonlinear Dyn.*, vol. 78, no. 4, pp. 2429–2438, 2014.
[28] S. Hahn, C. S. Morris, D. J. Bertges, and S. Wshah, "Deep learning for recognition of endoleak after endovascular abdominal aortic aneurysm repair," in *Proc. IEEE 16th Int. Symp. Biomed. Imag. (ISBI)*, Apr. 2019, pp. 759–763.

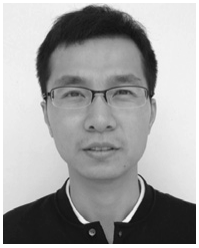

**XIAOGANG REN** received the B.S. degree in electronic information engineering from Jiangnan University, in 2003, and the M.S. degree in computer technology from the East China University of Technology, in 2016. His research interests include 3D reconstruction and 3D printing, medical image segmentation, and machine learning.

**YUE WU** received the B.S. degree in computer science from Jiangsu Technical Normal University, in 2008. Her research interests include network management and security and computer graphics and, medical image processing.

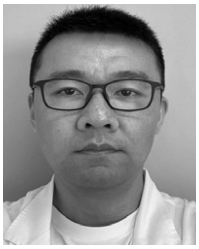

**LEI WANG** received the bachelor's degree in medicine from Nanjing Medical University, in 2003, and the master's degree in general surgery, in 2007. He is currently with the General Surgery Department, Affiliated Changshu Hospital, Soochow University, Jiangsu.

**XIAOQIANG YAN** received the B.S. degree in public service management from Nantong University, in 2010. He is currently with Affiliated Changshu Hospital, Soochow University. His research interests include medical informatics and electronic health archives.

**LI ZHANG** received the B.S. degree from the Changshu Institute of Technology. He is currently with Affiliated Changshu Hospital, Soochow University. His research interests include hospital information management, digital image processing, and 3D printing.

**ZHIYING CAO** received the B.S. degree in communication engineering from the Zijin College, in 2009. She is currently pursuing the M.S. degree with the East China University of Technology. Her research interests include medical image segmentation and machine learning.

**HUANGXING LIN** received the B.S. degree in tracking technology and instrument from Beijing Jiaotong University, in 2015, and the M.S. degree in control theory and control engineering from Xiamen University, Xiamen, China, in 2018, where he is currently pursuing the Ph.D. degree in signal and information processing. His research interests include MRI reconstruction, medical image segmentation, and machine learning.